

Anatase TiO₂ Nanowires Functionalized by Organic Sensitizers for Solar Cells : A Screened Coulomb Hybrid Density Functional Study

Hatice Ünal,¹ Deniz Gunceler,² Oğuz Gülseren,³ Şinasi Ellialtıoğlu,⁴ and Ersen Mete^{1,*}

¹*Department of Physics, Balıkesir University, Balıkesir 10145, Turkey*

²*Department of Physics, Cornell University, Ithaca, NY 14853, USA*

³*Department of Physics, Bilkent University, Ankara 06800, Turkey*

⁴*Basic Sciences, TED University, Ankara 06420, Turkey*

(Dated: February 28, 2022)

The adsorption of two different organic molecules cyanidin glucoside (C₂₁O₁₁H₂₀) and TA-St-CA on anatase (101) and (001) nanowires have been investigated using the standard and the range separated hybrid density functional theory calculations. The electronic structures and optical spectra of resulting dye-nanowire combined systems show distinct features for these types of photochromophores. The lowest unoccupied molecular orbital of the natural dye cyanidin glucoside is located below the conduction band of the semiconductor while, in the case of TA-St-CA, it resonates with the states inside the conduction band. The wide-bandgap anatase nanowires can be functionalized for solar cells through electron-hole generation and subsequent charge injection by these dye sensitizers. The intermolecular charge transfer character of Donor- π -Acceptor type dye TA-St-CA is substantially modified by its adsorption on TiO₂ surfaces. Cyanidin glucoside exhibits relatively stronger anchoring on the nanowires through its hydroxyl groups. The atomic structures of dye-nanowire systems re-optimized with the inclusion of nonlinear solvation effects showed that the binding strengths of both dyes remain moderate even in ionic solutions.

PACS numbers: 71.15.Mb, 68.47.Gh

I. INTRODUCTION

The wide bandgap metal oxide, TiO₂ has gained an increased attention since the discovery of its ability to carry out hydrolysis under UV irradiation by Fujishima and Honda.[1–7] In addition to showing such an excellent photocatalytic performance, TiO₂ has also become the material of choice as the anode in dye sensitized solar cell (DSSC) applications due to its favorable electrochemical and charge carrier conduction properties.[8–10]

In terms of more efficient utilization, titania possesses particularly importance with its nanocrystalline forms.[11–14] Quasi-one-dimensional TiO₂ nanostructures offer high surface-to-volume ratios that is desirable to improve efficiencies of photovoltaic and photocatalytic processes.[16–18]

The (001) and (101) terminations of the anatase polymorph are known to exhibit remarkably higher photocatalytic activity relative to the surfaces of the rutile phase.[19–22] Moreover, the naturally occurring anatase form has been reported to be the most stable phase of TiO₂ in nanodimensions.[11–14]

In a basic DSSC operation, many processes take place influencing overall device performances. These are the electron-hole generation upon visible light absorption by the dye sensitizer, the charge carrier injection from the dye to the conduction band (CB) of the oxide electrode, regeneration of the ground state of the dye by a redox reaction through liquid iodide/triiodide electrolytes.[8, 10]

Here one of the main concerns is the reduction of photogenerated electron-hole recombination rate. Another point is the binding strength of the sensitizer molecule to the oxide and the reliability of this system in the ionic solvent. Therefore, the type of the dye molecule and the surface properties of the semiconductor plays a key role in the optimization of such processes.

Recent experiments have shown that one-dimensional nanostructures have several advantages over nanoparticulate TiO₂ films.[12, 15] First of all they have higher surface-to-volume ratios allowing many active sites to come into contact with light harvesting molecules. Secondly, their one-dimensionality forms a natural pathway for the charge carrier conduction from the point of injection to the anode. Moreover, nanowires or nanotubes can exhibit a band transport rather than a hopping mechanism between nanoparticles. Another crucial aspect is that the electron-hole recombination rates were observed to be ten times lower in nanotube-based films in comparison with films made from nanoparticles.[15]

One of the key issues in DSSC is the type of the sensitizer dye and its interaction with the TiO₂ nanostructures. Commercially available Ru-based molecular complexes have shown up to 11% solar energy conversion efficiencies.[8, 23–30] These metal-driven dyes can perform spatial charge separation and fast injection rates. Meanwhile, researchers have also focused on finding natural alternatives. Recently, antenna type novel organic donor- π -acceptor (D- π -A) dyes have been proposed as sensitizers to achieve charge transfer excitations reducing recombination rates that is the basic concern in simple skeleton light harvesting molecules. For instance, π -conjugated organic complexes with tetrahydroquinoline

* emete@balikesir.edu.tr; Corresponding author

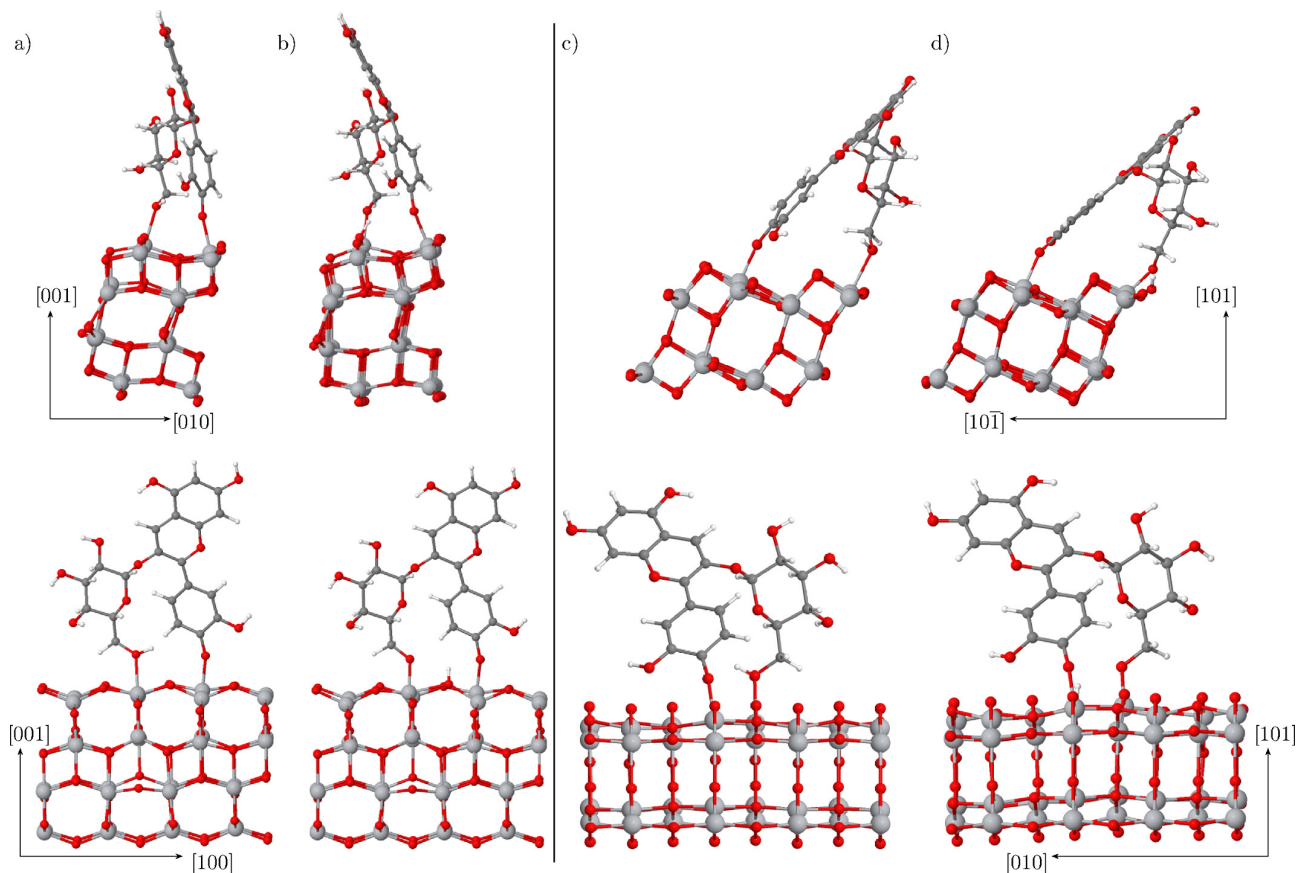


FIG. 1. Optimized adsorption geometries of cyanidin glucoside on anatase (001)-nanowire and (101)-nanowire

moiety as donor and a cyanoacrylic acid moiety as the acceptor were experimentally synthesized and theoretically studied.[31–34] From this class, a highly efficient organic dye, TA-St-CA, contains a π -conjugated oligophenylenevinylene electron donor–acceptor moiety and a carboxyl group as anchoring group.[35–41] Hwang *et al.* achieved % 9.1 photo-to-electric conversion efficiency with an open circuit voltage of 743 mV by designing a low cost TA-St-CA based DSSC.[35]

Natural dye pigments with a simple carbon skeleton structures such as cyanidin dyes are eco-friendly, widely available and cheap to produce. For instance, anthocyanin (cyanidin-3-O-glucoside) can easily be extracted from plants.[42] The cyanidin family is well known and is proposed as an alternative to other dye sensitizers.[42–69] However, reports indicate the overall solar-to-electric energy conversion efficiencies below the current requirements. A deeper understanding of the bottlenecks in their DSSC applications is still needed.

In this study, we theoretically investigated the adsorption modes, electronic structures and absorption spectra of two different types of dyes on anatase TiO_2 nanowires having (001) and (101) facets. For this reason, we considered the D- π -A type organic complex TA-St-CA and the natural chromophore anthocyanin as dye sensitizers. We used both the standard and the screened exchange

hybrid density functional theory (DFT) calculations to shed light on the main differences between the resulting nw+dye combined systems in vacuum as well as in solution treated with a modern nonlinear polarizable continuum model (PCM).

II. COMPUTATIONAL DETAILS

The DFT calculations have been performed using the projector-augmented wave (PAW) method[70] as implemented in the Vienna *ab-initio* simulation package (VASP).[71, 72] Single particle electronic states have been expanded using plane wave basis sets up to a kinetic energy cutoff value of 400 eV. We used the standard generalized gradient approximation (GGA) to describe the exchange–correlation (XC) effects with the semicolon Perdew–Burke–Ernzerhof (PBE)[73] functional as well as the contemporary hybrid XC functional proposed by Heyd–Scuseria–Ernzerhof (HSE).[74–76] The latter is a nonlocal, screened Coulomb potential scheme with a range-separation. HSE functional largely heals the inherent bandgap underestimation of the standard DFT. To do so, HSE[74–76] proposed to partially admix the exact Fock and the PBE exchange energies in the short

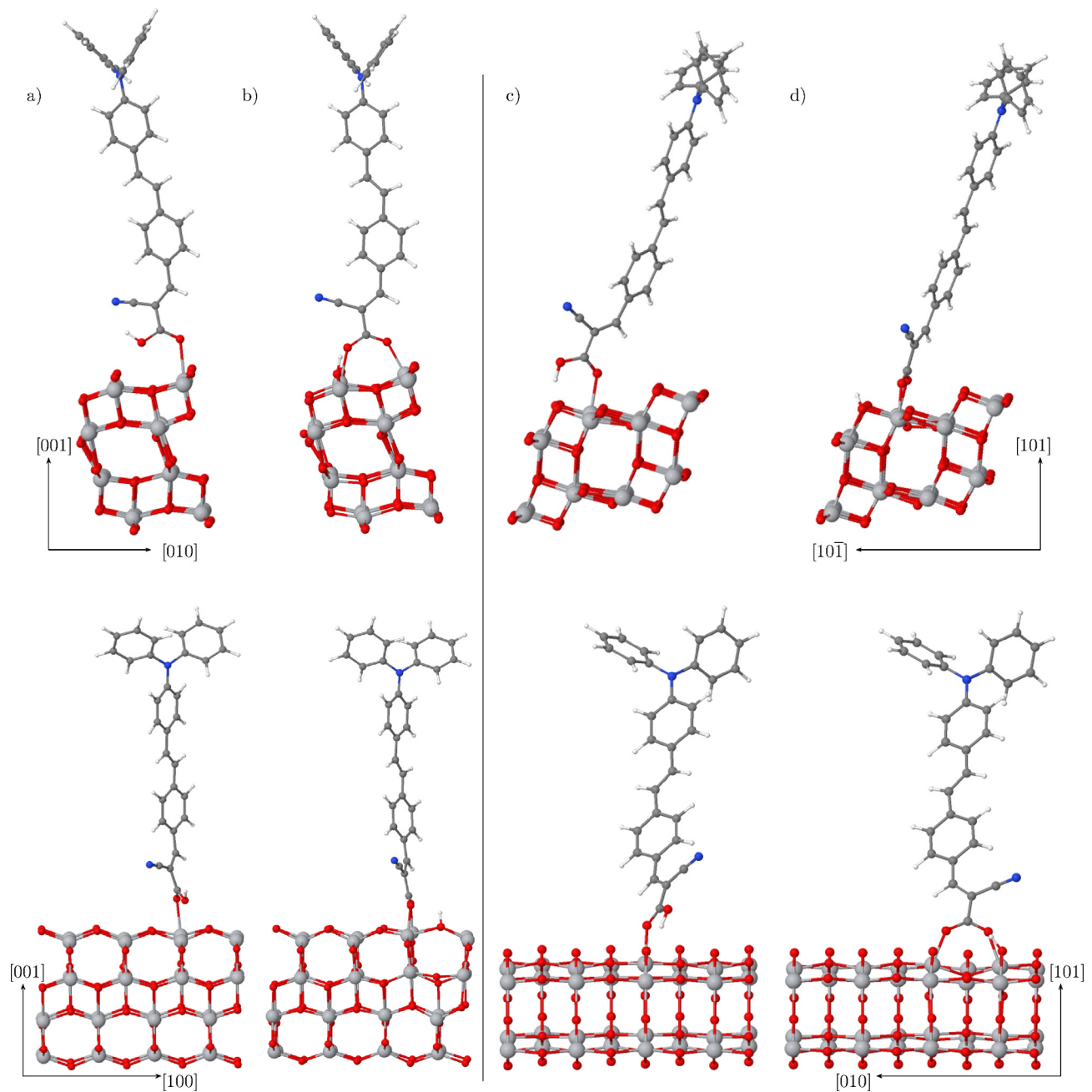


FIG. 2. Optimized adsorption geometries of TA-St-CA on anatase (001)-nanowire and (101)-nanowire

range (SR) part as

$$E_{\mathbf{x}}^{\text{HSE}} = aE_{\mathbf{x}}^{\text{HF,SR}}(\omega) + (1 - a)E_{\mathbf{x}}^{\text{PBE,SR}}(\omega) + E_{\mathbf{x}}^{\text{PBE,LR}}(\omega)$$

where a is the mixing coefficient [79] and ω is the range separation parameter.[74–76] Meanwhile, the long range (LR) part of the PBE exchange and the full PBE correlation energies are included in the HSE functional. In this way, the lack of proper self-interaction cancellation between the Hartree and exchange terms of the standard DFT is partly avoided leading to a substantial correction of the bandgap underestimation. In addition, the tendency of the standard DFT to give overly delocal-

ized charge density distributions is also corrected to some extent. Therefore, this range separated hybrid density functional approach not only improves the bandgap related properties over the standard exchange–correlation (XC) schemes but also offers a better description of localized states such as the Ti 3*d* states of TiO₂ or isolated gap states caused by various impurity atoms.[77, 78] Hence, the HSE functional offers an improvement over PBE-calculated electronic and optical properties while the difference in the optimization of lattice structures is relatively less recognizable between PBE and HSE calculations. In fact, for dye+nanowire systems considered

in this work, both XC functionals gave similar relaxed geometries and binding modes.

In order to obtain absorption spectra as the imaginary part of the dielectric function, $\varepsilon_2(\omega)$, from a density functional calculation, one considers the transitions from occupied to unoccupied states within the first Brillouin zone as the sum,

$$\varepsilon_{\alpha\beta}^{(2)}(\omega) = \frac{4\pi^2 e^2}{\Omega} \lim_{q \rightarrow 0} \frac{1}{q^2} \sum_{c,v,\mathbf{k}} 2w_{\mathbf{k}} \delta(\epsilon_{c\mathbf{k}} - \epsilon_{v\mathbf{k}} - \omega) \times \langle u_{c\mathbf{k}+\mathbf{e}_{\alpha q}} | u_{v\mathbf{k}} \rangle \langle u_{c\mathbf{k}+\mathbf{e}_{\beta q}} | u_{v\mathbf{k}} \rangle^*$$

where the c and v show empty and filled states respectively, $u_{c\mathbf{k}}$ are the cell periodic part of the orbitals and $w_{\mathbf{k}}$ are the weight factors at each \mathbf{k} -point.[80]

The nw(001) and nw(101) nanowire models are constructed from the anatase TiO₂ bulk structures. They are considered in large tetragonal supercells with dye adsorbates such that the periodicity of the cell is chosen to be five times larger than one unit cell length along the nanowire axis to isolate the molecules from each other on the nanowires (as in Fig. 1 and Fig. 2). In order to avoid unphysical interactions between the periodic images of the dye+nw structures, the supercells contain at least 20 Å of vacuum separations along both of the lattice translation vectors perpendicular to the one along the nanowire axis. We fully optimized initial geometries by minimizing the Hellman–Feynmann forces on each ionic core to be less than 0.01 eV/Å based on the conjugate-gradients algorithm. None of the atoms were frozen to their bulk positions during these relaxation procedures. In this way, the bare nanowire models were previously shown to maintain the anatase structure without a major lattice distortion.[81]

The effect of the solvent environment on the electronic structure of the dye–nanowire composed systems has been studied using the nonlinear polarizable continuum model (PCM) as implemented in the open-source code JDFTx.[82–84] Since the nonlinear models incorporate the dielectric saturation effect, the nonlinear[82] PCMs are expected to be more accurate than similar linear models in the presence of highly polar structures such as TiO₂. In such models, the contribution to the dielectric function arising from the rotations of solvent molecules are modeled as a field of interacting dipoles, whose response function saturates with increasing external field. The cavity surrounding the solute is constructed self-consistently from its electron density, where the dielectric function of the solvent turns on at a critical electron density contour. The numerical value of the critical electron density and the effective surface tension of the solute–solvent interface are highly solvent dependent. For solvents composed of small and highly polar molecules (such as water), the effective surface tension at the interface is positive; whereas for solvents with large molecules and strong dispersion (van der Waals) interactions (such as chloroform) this effective tension often has a negative sign. Additional technical details on the

polarizable continuum model used as well as the numerical values for the critical electron densities and effective surface tensions of the solute–solvent interfaces can be found in the relevant publications.[82, 84, 85]

III. RESULTS & DISCUSSION

The natural dye (cyanidin 3-O-glucoside) has been considered as a sensitizer for DSSC applications by various groups.[42–69] The main advantages over the other organic dyes have been pointed out as the simple and low cost production together with its wide availability in nature. Theory based studies on this class of dyes are rather rare and mostly limited to isolated molecules in the gas phase. We considered various probable initial adsorption configurations of the cyanidin dye on both (001) and (101) anatase nanowire models. We carried out the full optimization of the atomic coordinates using both PBE and HSE functionals. Results indicate energetically favorable two different binding modes on both nanowires as shown in Fig. 1. In order to differentiate between these two modes we refer them as the physical and chemical bindings. In the physical binding, the tail oxygen of the cyanidin part and the oxygen of the OH group at the end of glucoside moiety interacts with two five-fold coordinated surface Ti atoms (see Fig 1a and Fig 1c). In the chemical binding mode, the OH group additionally loses its hydrogen to the nearest surface oxygen site on both nw(001) and nw(101) models as shown in Fig 1b and Fig 1d, respectively. Hence, the calculated adsorption energies presented in Table I indicate stronger binding for the latter one.

The HSE-calculated Ti–O bond lengths between the cyanidin dye and nw(001) are 2.04 Å (on the cyanidin part) and 2.22 Å (on the glucoside side) for the physical adsorption mode. The second bond shortens to 1.88 Å in the chemical binding case. On nw(101), the corresponding bonds are 2.35 Å and 1.99 Å for the physical binding while they are 1.97 Å and 1.91 Å for the chemical binding mode.

The geometry optimizations using the standard PBE and modern HSE functionals gave similar final structures except the chemical binding mode of cyanidin molecule on the (101) nanowire. PBE calculations predict much stronger interaction between the natural dye and the (101) surface of the oxide. The PBE functional leads to considerable local distortion around the adsorption site where the bond lengths abruptly change. For instance, PBE-relaxation breaks the bond between the surface Ti which the dye is anchored at and the adjacent surface O which captures the hydrogen from the dye. The separation between them increases from the typical surface O–Ti bond length of 1.97 Å to 3.81 Å. While PBE causes such a local reconstruction, HSE calculations yield an adsorption geometry where the (101) nanowire keeps its bare surface structure. Therefore, calculated binding energies for this case are 2.35 eV and 1.20 eV with PBE

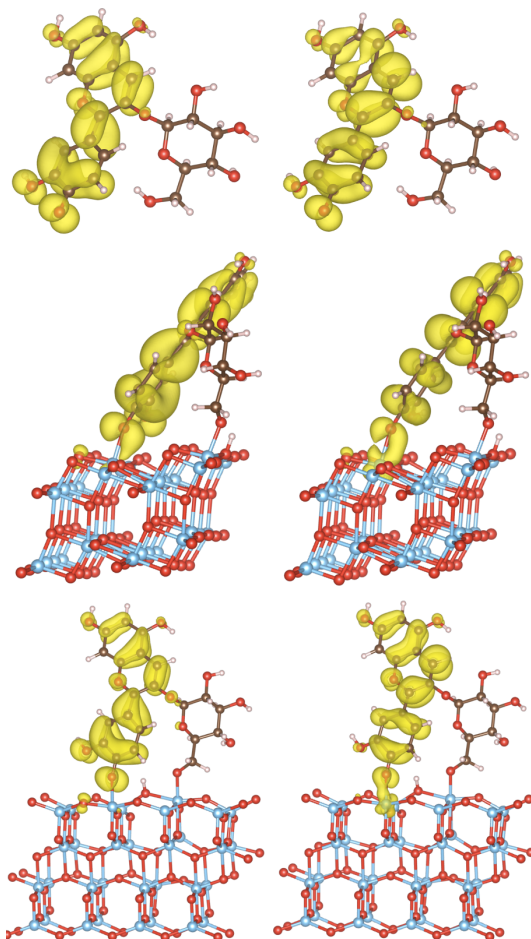


FIG. 3. Charge densities of the highest occupied states (on the left) and the lowest unoccupied states (on the right) of cyanidin glucoside dye (top row), dye+nw(101) (middle row), and dye+nw(001) (bottom row).

and HSE schemes, respectively (see Table I). Experimental studies does not report a binding at the chemisorption level to support the PBE predictions for this specific case. Therefore, this can be seen as one of the examples where the standard exchange–correlation functionals end up with peculiar results.

The TA-St-CA molecule on the (001) and (101) facets of the anatase nanowires has two different low energy adsorption structures, the monodentate and the bidentate binding modes as shown in Fig 2. The monodentate binding portrays perpendicular alignment with respect to the nanowire axis as a result of the single bond formation between the tail oxygen and surface Ti atom. The bidentate mode is similar to the cyanidin case because of the additional H transfer from the OH group at the tail to the nearest surface oxygen site on both of the nanowire types. The loss of hydrogen from the dye to the surface enables another O–Ti bond formation between the molecule and the oxide.

In the bidentate case, both O–Ti bonds are 2.01 Å be-

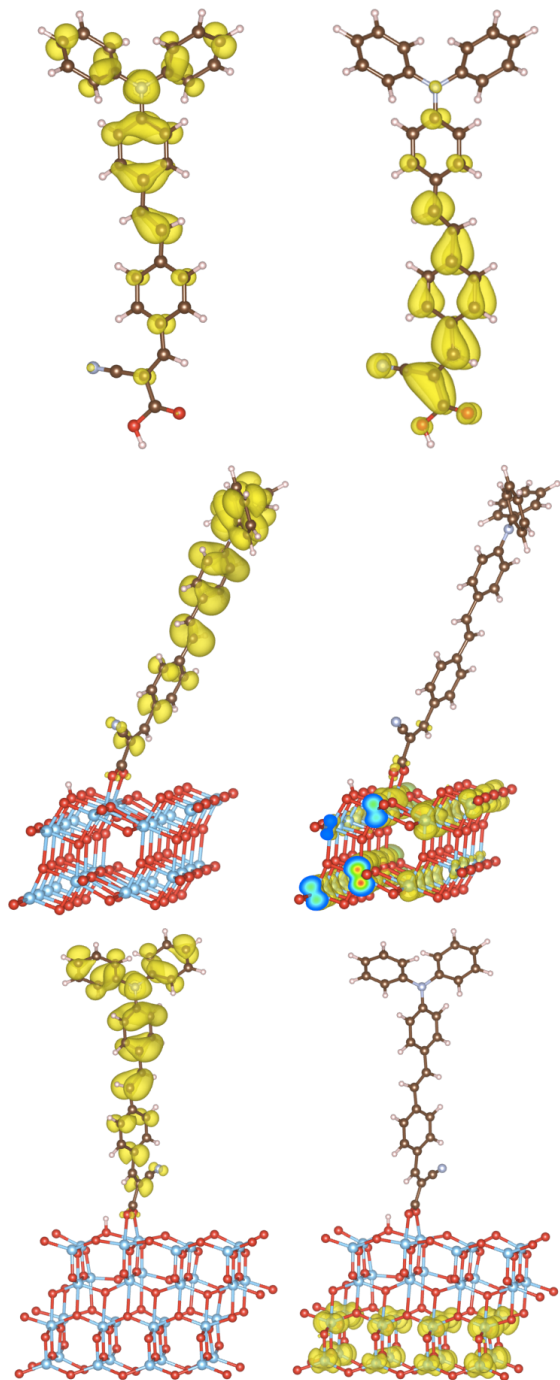


FIG. 4. Charge densities of the highest occupied states (on the left) and the lowest unoccupied states (on the right) of TA-St-CA dye (top row), dye+nw(101) (middle row), and dye+nw(001) (bottom row).

tween TA-St-CA and nw(101). Likewise, they are 2.03 Å on nw(001). Monodentate TA-St-CA forms a single bond of 2.14 Å on nw(101) while it is 2.36 Å on nw(001). These results expectedly indicate stronger binding in favor of the bidentate adsorption. A similar conclusion can be drawn from the calculated binding energies in Table I.

TABLE I. Calculated adsorption energies, E_{ads} , of the dye–nanowire systems

Dye	@ (001)				@ (101)			
	PBE	HSE	PBE+PCM ¹	PBE+PCM ²	PBE	HSE	PBE+PCM ¹	PBE+PCM ²
cyanidin glucoside (physical)	-1.35	-1.22	-1.13	-0.78	-1.47	-1.42	-1.16	-0.74
cyanidin glucoside (chemical)	-1.67	-1.30	-1.33	-0.89	-2.59	-1.20	-2.08	-1.44
TA-St-CA (monodentate)	-0.24	-0.28	-0.03	0.18	-0.74	-0.72	-0.50	-0.26
TA-St-CA (bidentate)	-1.05	-1.02	-0.81	-0.58	-0.84	-0.93	-0.64	-0.43

¹ in CH₃Cl using nonlinear PCM

² in H₂O using nonlinear PCM

Molecular complexes with anchoring groups are rather obvious to yield larger adsorption. However, the main difference between TA-St-CA and cyanidin dyes is not their sizes. The most important factor is that while TA-St-CA is specifically designed to do an intramolecular charge separation from the antenna part to the acceptor moiety which attaches to the oxide surface, both the HOMO and LUMO charge densities are localized on the cyanidin part of the cyanidin-3-O-glucoside. The glucoside group does not give any contribution to the frontier molecular orbitals in the case of cyanidin dye. This can be seen from the calculated charge density distributions for the corresponding states of the molecules in their gas phase as shown at the first rows of Fig 3 and Fig. 4.

In fact, the comparison of the charge density redistribution features for the lowest lying optical excitation becomes more important when these molecules are attached to the oxide surfaces. Therefore, the spatial charge densities of the highest occupied and the lowest unoccupied states of dye+nw combined systems have been calculated to discuss the charge injection features of these two different types of dyes. The HSE results are presented in the middle and at the bottom rows of Fig. 3 and Fig. 4 for the nw(101) and the nw(001) cases, respectively. The charge densities of the frontier molecular orbitals of the cyanidin dye remain very similar to their gas phase distributions even if it forms two O-Ti bonds with both the anatase (001) and (101) surfaces. These two states also appear in the band gap of nanowires as well-localized isolated states, one being filled and the other one being empty (see Fig. 5). Hence, the lowest vertical excitation does not involve a charge injection to the CB of the semiconductor. Such an excitation is prone to yield an electron–hole recombination. Therefore, HSE-calculated charge density results might partially explain why this type of natural dye pigments end up with relatively low incident photon to current efficiencies (IPCE).

The charge density distributions of the frontier orbitals of an isolated TA-St-CA molecule in vacuum have been investigated by Zhang *et al.*[37] and Mohammadi *et al.*[41] using hybrid DFT calculations. Their gas phase results agree with our calculations for the isolated molecule case as shown in the top row of Fig. 4. In the case of

TA-St-CA on TiO₂, the intramolecular charge transfer character from the triphenylamine part as donor to the cyanoacrylic acid group as the acceptor seems to be significantly altered after the molecule is adsorbed on the anatase nanowires. The lowest lying excitation involve a transition from the HOMO-like state which is spatially well-localized on the antenna moiety to the CB of the anatase as shown for the TA-St-CA+nw combined systems in Fig. 4. Therefore, our calculations indicate that upon adsorption the loss of donor- π -acceptor gas phase feature of TA-St-CA changes in favor of better charge injection into the CB of the oxide. This might also be interpreted as accounting for the reduction of recombination rates in the case of phenylenevinylene-conjugated D- π -A type sensitizers.

The adsorption energies of the molecules have been calculated using

$$E_{\text{ads}} = E_{\text{dye+nw}} - (E_{\text{dye}} + E_{\text{nw}})$$

where $E_{\text{dye+nw}}$, E_{dye} , and E_{nw} are the relaxed supercell energies of dye adsorbed nanowire, the isolated dye molecule, and the bare anatase nanowire, respectively. Both the PBE and HSE functionals were used for the vacuum calculations as presented in Table I. Then, we obtained adsorption energies in solution for chloroform and water using a new non-linear PCM[82] with the PBE functional. Our tests show that similar conclusions can be drawn when the solvent effects are included within the hybrid HSE scheme. The vacuum results with PBE and HSE functionals are only slightly different from each other except the chemical binding of the cyanidin dye on the nw(101). For this case, the energy difference of 1.39 eV is due to the fact that the PBE functional overestimates the bonding between the hydrogen atom captured from the dye with the nearest surface oxygen, which results in an additional local modification of atomic positions relative to the HSE-optimized structure where surface Ti-O row seems to be disturbed less.

As expected, single bond formation leads to a weaker adsorption energy for each type of dye. The loss of H from the OH group of the dye to the nearest surface oxygen causes the formation of a second bond. This situation enhances the binding appreciably, especially in

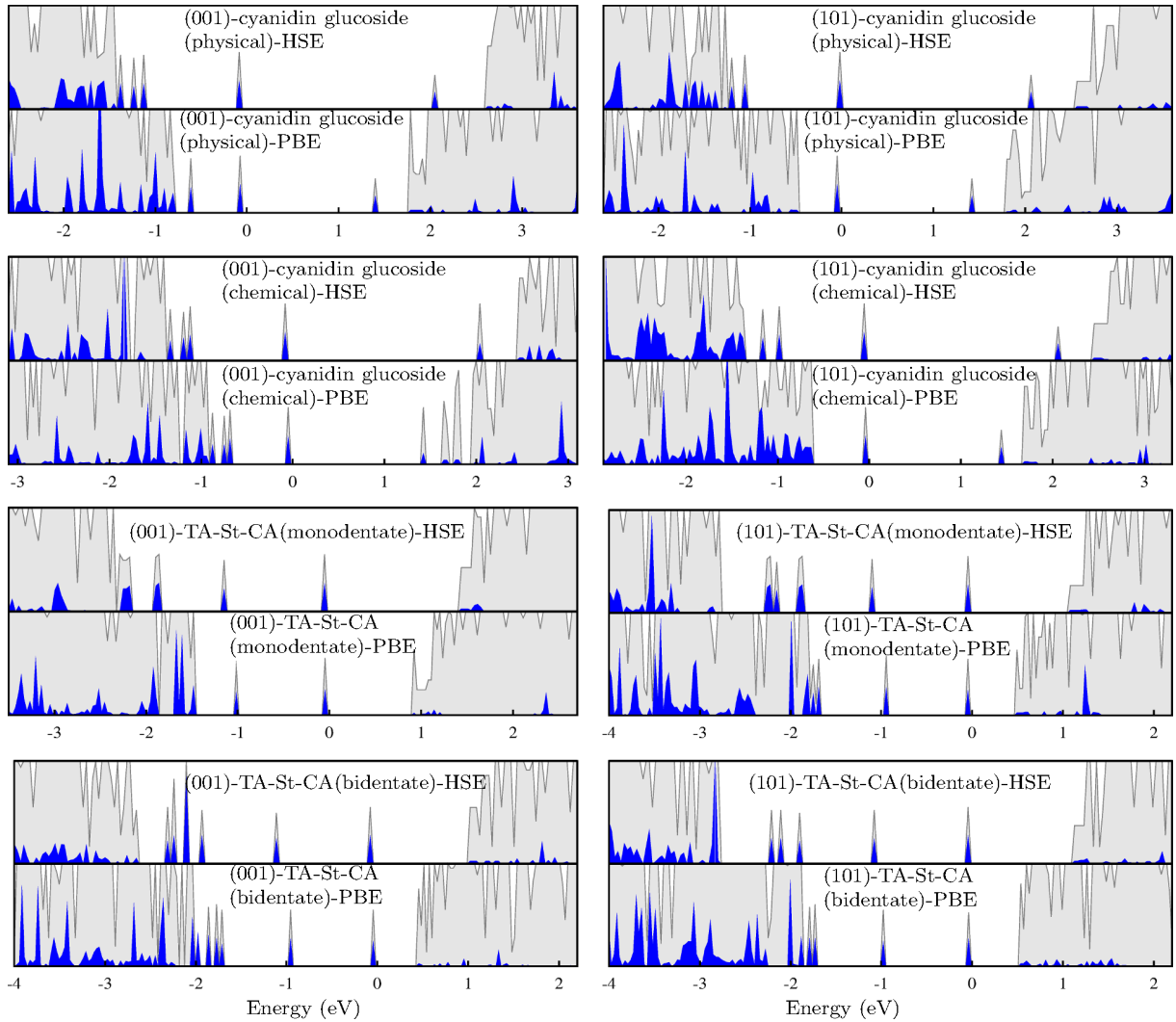


FIG. 5. Densities of states for the dye+nanowire systems (in arbitrary units) calculated using the PBE and HSE functionals. The partial DOS contributions of the dye molecules are shown as dark (blue) shades.

the bidentate mode of TA-St-CA. Clearly, the binding of the molecules appears to be noticeably stronger in vacuum. As a nonpolar solvent with a dielectric constant of 4.8, chloroform has a little effect on the adsorption energies. However, water, being a polar solvent, weakens the bond(s) between the dye and the nanowire, considerably. For instance, the results show that monodentate TA-St-CA is washed away from the surface. In the other cases, the dye molecules can keep moderate binding with the oxide even in water environment.

We note that the binding energies change in the positive direction as seen in Table I. The reason is that the binding sites on the TiO_2 nanowire and the dye molecule interact strongly with the solvent. On the other hand, such an interaction is absent in a vacuum calculation leading to a more negative binding energy. When we check the differences between the calculated Kohn-Sham eigenvalues in vacuum and in solution, we see that the energy levels are slightly shifted with respect to each other.

Since H_2O is a more polar solvent than CHCl_3 with a higher dielectric constant, it interacts more strongly with the binding sites; we therefore see that binding energies in H_2O are more positive than the binding energies in CHCl_3 .

Since the dye molecules develop a bonding interaction with the oxide surface, dye-related HOMO-like levels appear in the band gap of the oxide as isolated and well-localized states. In addition, their LUMO levels show a strong dispersion inside the CB of TiO_2 . Those can no longer be considered as molecular energy levels. Therefore an optical excitation starts from the HOMO-like dye-related state to the states in the CB.

For an efficient DSSC, the lowest lying absorption peaks (in the visible range) mainly involve transitions from the HOMO-like dye-related states which appear above the VB to the states in the CB of TiO_2 . If the dye molecules had broken apart and been dissolved in solution one could have expected the loss of main fea-

tures of the absorption peaks. However, we have shown that the water or chloroform can only weaken the bonds between the molecules and TiO_2 . When we check the differences between the calculated Kohn–Sham eigenvalues in vacuum and in solution, we see that the single particle energy levels are slightly shifted with respect to each other. Therefore, from a theoretical point of view, the difference in the calculated electronic properties between the standard PBE and modern HSE exchange–correlation schemes is much larger than the energy shifts due to PCM.

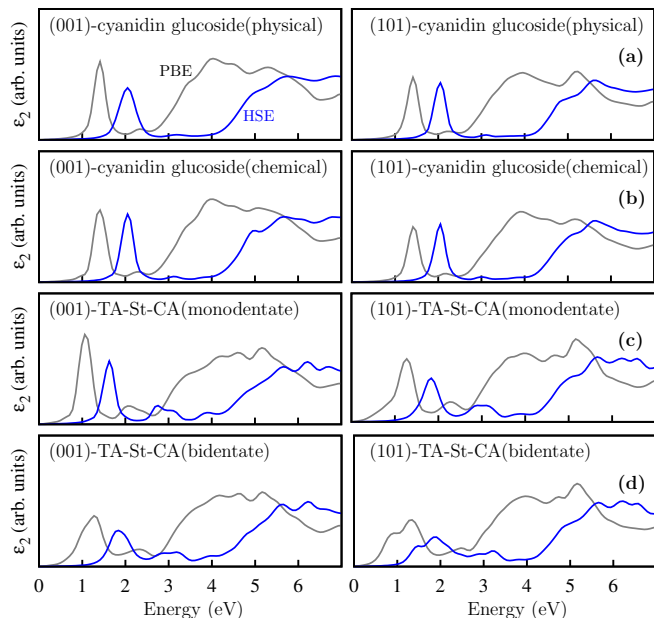


FIG. 6. First two rows display the calculated absorption spectra of the dye+nanowire combined systems : (a) physical (b) chemical binding of cyanidin glucoside on the anatase nw(001) and nw(101), respectively. The last two rows show the absorption spectra for (c) monodentate TA-St-CA and (d) bidentate TA-St-CA on anatase nw(001) and nw(101), respectively.

In order to discuss the electronic structures of the dye+nanowire combined systems the partial density of states has been calculated for each binding mode using both the PBE and HSE functionals as presented in Fig. 5. Since, the DOS structures calculated using the PBE and HSE functionals were aligned with respect to their deep core states, the HSE VB edge lies lower than the PBE one. Therefore, in the case of HSE, several new dye-related states fall in the band gap, which seem to occupy the top of the VB in the PBE DOS structures. The inclusion of partial short ranged exact exchange corrects the description of Ti $3d$ states reasonably. Since the CB of TiO_2 is composed of these d bands, the CB gets shifted up to higher energies. Therefore, HSE functional heals the band gap underestimation of the standard exchange–correlation schemes not only by shifting up of the CB edge but also by lowering the VB edge. Meanwhile, the presence of new dye related gap states cause a signifi-

cant narrowing of the band gap, which functionalizes the combined system to be active in the visible region.

The absorption spectra of the dye+nanowire systems have been obtained at the PBE and HSE levels by calculating the dipole transition matrix elements between the occupied and the empty states. Similar computations were performed previously for the bare anatase nanowires.[34] The presence of new isolated and occupied gap states originating from the dye adsorbates just above the VB edge of the oxide is desirable for functionalization of TiO_2 in the visible part of the spectrum. When one compares the calculated optical spectra, similarities can be found between the two nanowire types as well as between the results of PBE and HSE functionals as shown in Fig. 6. Among these characteristics, the first absorption peaks in each case are associated with the vertical transitions from the dye-related HOMO-like gap states to the lowest lying unoccupied states. Those sharp peaks indicate a significant red shift of the absorption threshold into the visible region which is favorable for titania based photovoltaic applications. Although the overall features look alike, PBE-calculated spectra is also considerably red shifted relative to those of the HSE due to the local density approximation (LDA) to exchange–correlation effects giving rise to an underestimation of the band gap of TiO_2 . Moreover, the red shifting of the PBE spectra with respect to the HSE results gets even larger for the higher lying transitions.

Experimentally, Senthil *et al.*[42] reported the first absorption peak of cyanidin-3-O-glucoside adsorbed on TiO_2 nanoparticles at 2.22 eV. Although the efficiency they have obtained with this dye is still below the requirements as they said, the main reason remained unclear. In our calculation for the cyanidin glucoside on both of the nanowire types, the first absorption peak positions are found around 1.5 eV and 2.2 eV with PBE and HSE functionals, respectively, which coincide with the energy difference between the isolated dye-related gap states as seen in the top two panels of Fig. 5. Therefore, the lowest lying transitions in each case essentially involve an intramolecular excitation from the HOMO-like state to the LUMO-like state in the band gap as seen in first two panels of Fig. 5. The corresponding charge density distributions can also be seen in Fig. 3. Although the first absorption peak seems to drive the photoresponse of the combined system to visible region, the associated excitation takes place on the dye itself without any sign of charge injection into the semiconductor. This might be seen as one of the factors why these type of natural dyes have relatively low incident photon to current efficiency (IPCE) observed in experiments.[42]

Recently, Hwang *et al.* reported an overall solar-to-energy conversion efficiency of 9.1 % with TA-St-CA sensitizer.[35] The experimental optical absorption peaks were found around 2.4 eV.[35, 36] This value agrees with our HSE results for the bidentate TA-St-CA. The remarkable difference in the efficiencies between the natural cyanidin and organic TA-St-CA sensitizers needs an

understanding from a theoretical perspective. First of all, the adsorption of TA-St-CA causes the LUMO to resonate with the Ti 3*d* states and get delocalized in the CB of the anatase nanowires. Therefore, the first peaks corresponding to absorption in the visible region are due to transition from the dye-related HOMO-like gap states to the states in the CB as seen in the bottom two panels of Fig. 6. The inclusion of screened exact exchange in the HSE functional shifts the CB edge to higher energies such that the gap values become ~ 1.3 eV whereas the PBE gaps are considerably underestimated as seen in Fig. 5. Consequently, the first peak positions agree with the energy difference of those states involved in the transition. When we look at the corresponding charge density plots in Fig. 4, we see a charge injection into the oxide through electron-hole generation upon visible light absorption. In comparison to the cyanidin case, the appearance of a group of dye-related states just above the VB edge in the HSE results translates into an absorption ability of the TA-St-CA+nanowire system in a wider range of the visible spectrum with varying oscillator strengths. For the TA-St-CA sensitizer, transitions might arise from these group of gap states below the HOMO-like level to the states in the CB causing shallow peaks around 3 eV shown in Fig. 6c and d. The results indicate that the cyanidin dye is not successful in sensitizing anatase nanowires in the region between the first peaks and the main body of the higher energy contributions. This is much more pronounced in the spectra obtained with HSE functional. Higher frequency contributions to absorption in the UV part of the spectrum are mostly associated with the interband transitions from the states in the VB to the states in the CB of the dye+nanowire system. Both molecules bring the lowest lying peak which drops the absorption threshold into the visible region as seen in Fig. 6 for both nanowire types. The TA-St-CA+nanowire combined system has more favorable optical properties than the cyanidin glucoside+nanowire structure.

IV. CONCLUSIONS

The natural chromophore cyanidin-3-O-glucoside and the D- π -A type organic dye TA-St-CA have been separately considered on anatase TiO₂ nanowires having either (101) or (001) facets. The standard and the screened Coulomb hybrid density functional theory calculations were performed to understand the adsorption modes, electronic structures and absorption spectra of dye+nanowire combined systems. The binding energies have been obtained in vacuum and in solution using a new non-linear PCM. Our results indicate a significant band gap narrowing upon adsorption on both of the nanowire facets due to the appearance of a number of isolated dye-related gap states. Their number increases when a second bond is formed between the dye molecule

and the oxide. The HSE-calculated VB edge lies energetically lower with respect to that obtained using the PBE functional. This causes several dye-related states to fall in the band gap just above VB. Therefore, the HSE functional gives a larger number of occupied gap states. In addition, the HSE functional corrects the band gap underestimation of the standard approximations to the exchange-correlation energy by admixing partial screened exact exchange. Therefore, unoccupied Ti 3*d* states are better described with the HSE functional leading to a significant shift of the CB up to higher energies.

The cyanidin dye can form single and double bonds through its tail oxygens with the surface Ti ions on anatase. The latter is a chemical binding where the nearest surface oxygen captures an H from the tail OH group of cyanidin dye. Both adsorption modes bring several new occupied states above the VB and an empty state below the CB of TiO₂ at both the PBE and the HSE levels of theory. The lowest lying transition starting from the HOMO-like dye-related gap state to the empty LUMO-like state below the CB takes place on the dye itself giving a sharp absorption peak in the visible range. This can be understood as a factor limiting a subsequent charge injection into the nanowire and might end up with recombination of photoexcited electron-hole pairs. TA-St-CA shows mono- and bidentate binding modes on both of the anatase nanowires. When adsorbed, its intramolecular charge transfer character gets favorably modified toward a charge injection into the oxide. This might help reduce the recombination rates of charge carriers. The isolated filled gap states originating from the bidentate binding of TA-St-CA sensitizer significantly narrow the energy gap and effectively functionalize the anatase nanowires to actively absorb a broader range of the visible spectrum. Inclusion of nonlinear solvation effects indicates dissociation of the monodentate TA-St-CA from the nanowires in water where the bidentate TA-St-CA develops a moderate binding. In a more polar ionic solution, TA-St-CA needs a firmer anchoring to the oxide. Although the cyanidin molecule has a strong binding on the (101) and (001) nanowires even in an electrolyte, the absorption properties are weaker and might suffer from recombination of photogenerated electron-hole pairs. Bidentate TA-St-CA+nanowire systems can achieve directional charge transfer excitation to increase charge injection probabilities, allow absorption in the wide range of visible spectrum with enhanced light harvesting, and exhibit moderate binding in solution required to reduce degradation of possible device operation.

ACKNOWLEDGMENTS

This work was supported by TÜBİTAK, The Scientific and Technological Research Council of Turkey (Grant #110T394). Computational resources were provided by ULAKBİM, Turkish Academic Network and Information Center.

- [1] A. Fujishima and K. Honda, *Nature (London)* **238**, 37 (1972).
- [2] U. Diebold, *Surf. Sci. Rep.* **48**, 53 (2003).
- [3] S. Khan, J. M. Al-Shahry, and W. B. Ingler, *Science* **297**, 2243 (2002).
- [4] M. Chen, Y. Cai, Z. Yan, and D. W. Goodman, *J. Am. Chem. Soc.* **128**, 6341 (2006).
- [5] W. G. Zhu, X. F. Qiu, V. Iancu, X. Q. Chen, H. Pan, W. Wang, N. M. Dimitrijevic, T. Rajh, H. M. Meyer, M. P. Paranthaman, G. M. Stocks, H. H. Weiering, B. H. Gu, G. Eres, and Z. Y. Zhang, *Phys. Rev. Lett.* **103**, 226401 (2009).
- [6] W.-J. Yin, H. Tang, Su-H. Wei, M. M. Al-Jassim, J. Turner, and Y. Yan, *Phys. Rev. B* **82**, 045106 (2010).
- [7] V. Çelik, H. Ünal, E. Mete, and Ş. Ellialtıođlu, *Phys. Rev. B* **82**, 205113 (2010).
- [8] B. O'Regan and M. Grätzel, *Nature (London)* **353**, 737 (1991).
- [9] A. Hangfeldt and M. Grätzel, *Chem. Rev.* **95**, 49 (1995).
- [10] M. Grätzel, *Nature (London)* **414**, 338 (2001).
- [11] P. K. Naicker, P. T. Cummings, H. Zhang, and J. F. Banfield, *J. Phys. Chem. B* **109**, 15243–15249 (2005).
- [12] J. E. Boercker, E. Enache-Pommer, and E. S. Aydil, *Nanotechnology* **19**, 095604 (2008).
- [13] A. Iacomino, G. Cantele, F. Trani, and D. Ninno, *J. Phys. Chem. C* **114**, 12389–12400 (2010).
- [14] V. C. Fuertes, C. F. A. Negre, M. B. Oviedo, F. P. Bonafé, F. Y. Oliva, and C. G. Sánchez, *J. Phys.: Condens. Matter* **25**, 115304 (2013).
- [15] K. Zhu, N. R. Neale, A. Miedaner, and A. J. Frank, *Nano Lett.* **7**, 69–74 (2007).
- [16] X. Chen and S. S. Mao, *Chem. Rev.* **107**, 2891 (2007).
- [17] D. Çakır and O. Gülsereen, *J. Phys.: Condens. Matter* **24**, 305301 (2012).
- [18] D. Çakır and O. Gülsereen, *Phys. Rev. B* **80**, 125424 (2009).
- [19] R. Hengerer, B. Bolliger, M. Erbudak, and M. Grätzel, *Surf. Sci.* **460**, 162–169 (2000).
- [20] M. Lazzeri, A. Vittadini, and A. Selloni, *Phys. Rev. B* **63**, 155409 (2001).
- [21] A. G. Thomas, W. R. Flavell, A. R. Kumarasinghe, A. K. Mallick, D. Tsoutsou, and G. C. Smith, *Phys. Rev. B* **67**, 035110 (2003).
- [22] A. Selloni, *Nat. Mater.* **7**, 613 (2008).
- [23] M. K. Nazeeruddin, A. Kay, I. Rodicio, R. Humphry-Baker, E. Müller, P. Liska, N. Vlachopoulos, and M. Grätzel, *J. Am. Chem. Soc.* **115**, 6382 (1993).
- [24] Y. Tachibana, J. E. Moser, M. Grtzel, D. R. Klug, and J. R. Durrant, *J. Phys. Chem.* **100**, 20056–20062 (1996).
- [25] D. W. Thompson, J. F. Wishart, B. S. Brunshwig, and N. Sutin, *J. Phys. Chem. A* **105**, 8117 (2001).
- [26] S. Nakade, W. Kubo, Y. Saito, T. Kamzaki, T. Kitamura, Y. Wada, and S. J. Yanagida, *J. Phys. Chem. B* **107**, 14244 (2003).
- [27] P. Wang, S. M. Zakeeruddin, J. E. Moser, M. K. Nazeeruddin, T. Sekiguchi, and M. Grätzel, *Nat. Mater.* **2**, 402 (2003).
- [28] G. Benkö, J. Kallioinen, P. Myllyperkiö, F. Trif, J. E. I. Korppi-Tommola, A. P. Yartsev, and V. Sundström, *J. Phys. Chem. B* **108**, 2862–2867 (2004).
- [29] P. Wang, C. Klein, R. Humphry-Baker, S. Zakeeruddin, and M. Grätzel, *Appl. Phys. Lett.* **86**, 123508 (2005).
- [30] M. K. Nazeeruddin, F. De Angelis, S. Fantacci et al. *J. Am. Chem. Soc.* **127**, 16835 (2005).
- [31] R. Chen, X. Yang, H. Tian, X. Wang, A. Hagfeldt, and L. Sun, *Chem. Mater.* **19**, 4007–4015 (2007).
- [32] R. Chen, X. Yang, H. Tian, and L. Sun, *J. Photochem. Photobiol. A: Chemistry* **189** 295–300 (2007).
- [33] C. O'Rourke and D. R. Bowler, *J. Phys. Chem. C* **114**, 20240–20248 (2010).
- [34] H. Ünal, Deniz Gunceler, O. Gülsereen, Ş. Ellialtıođlu, and E. Mete, *J. Phys. Chem. C*, **118**, 24776–24783 (2014).
- [35] S. Hwang, J. H. Lee, C. Park, H. Lee, C. Kim, C. Park, M.-H. Lee, W. Lee, J. Park, K. Kim, N.-G. Park, and C. Kim, *Chem. Commun.* 4887–4889 (2007).
- [36] G.-W. Lee, D. Kim, M. J. Ko, K. Kim, and N.-G. Park, *Solar Energy* **84**, 418–425 (2010).
- [37] C.-R. Zhang, Z.-J. Liu, Y.-H. Chen, H.-S. Chen, Y.-Z. Wu, W.J. Feng, and D.-B. Wang, *Current Appl. Phys.* **10**, 77–83 (2010).
- [38] F. Yang, M. Akhtaruzzaman, A. Islam, T. Jin, A. El-Shafei, C. Qin, L. Han, K. A. Alamry, S. A. Kosa, M. A. Hussein, A. M. Asirie, and Y. Yamamoto, *J. Mater. Chem.* **22**, 22550–22557 (2012).
- [39] G. Liang, J. Xu, W. Xu, L. Wang, X. Shen, and M. Yao, *Bull. Korean Chem. Soc.* **32**, 2279 (2011).
- [40] G. D. Sharma, S. P. Singh, P. Nagarjuna, J. A. Mikroyannidis, R. J. Ball, and R. Kurchania, *J. Renewable Sustainable Energy* **5**, 043107 (2013).
- [41] N. Mohammadi, P. J. Mahon, and F. Wang, *J. Molecular Graphics and Modelling* **40**, 64–71 (2013).
- [42] T.S. Senthil, N. Muthukumarasamy, D. Velauthapillai, S. Agilan, M. Thambidurai, and R. Balasundaraprabhu, *Renewable Energy* **36**, 2484–2488 (2011).
- [43] K. Tennakone, G. R. R. A. Kumara, A. R. Kumarasinghe, K. G. U. Wijayantha, and P. M. Sirimanne, *Semicond. Sci. Technol.* **10**, 1698 (1995).
- [44] N. J. Cherepy, G. P. Smestad, M. Grätzel, and J. Z. Zhang, *J. Phys. Chem. B* **101**, 9342–9351 (1997).
- [45] A. Ehret, L. Stuhl, and M.T. Spitler, *J. Phys. Chem. B* **105**, 9960–9965 (2001).
- [46] F. C. Stintzing, A. S. Stintzing, R. Carle, B. Frei, and R. E. Wrolstad, *J. Agric. Food Chem.* **50**, 6172 (2002).
- [47] Q. Dai and J. Rabani, *J. Photochem. Photobiol. A* **148**, 17–24 (2002).
- [48] W. Zheng and Y. Wang, *J. Agric. Food Chem.* **51**, 502 (2003).
- [49] J.-M. Kong, L.-S. Chia, N.-K. Goh, T.-F. Chia, and R. Brouillard, *Phytochem.* **64**, 923 (2003).
- [50] F. Galvano, L. La Fauci, G. Lazzarino, V. Fogliano, A. Ritieni, S. Ciappellano, N. C. Battistini, B. Tavazzi, and G. Galvano, *J. Nutr. Biochem.* **15**, 2 (2004).
- [51] S. Hao, J. H. Wu, Y. F. Huang, and J. M. Lin, *Sol. Energy* **80**, 209–214 (2006).
- [52] T. K. McGhie, D. R. Rowan, and P. J. Edwards, *J. Agric. Food Chem.* **54**, 8756 (2006).
- [53] J. Parry, L. Su, J. Moore, Z. Cheng, M. Luther, J. N. Rao, J.-Y. Wang, and L. L. Yu, *J. Agric. Food Chem.* **54**, 3773 (2006).
- [54] P. M. Sirimanne, M. K. I. Senevirathna, E. V. A. Premalal, P. K. D. D. P. Pitigala, V. Sivakumar, and K. J.

- Tennakone, *Photochem. Photobiol. A* **177**, 324 (2006).
- [55] A.S. Polo and N.Y. Murakami Iha, *Sol. Energy Mater. Sol. C* **90**, 1936–1944 (2006).
- [56] J. He, E. Rodriguez-Saona, and M. M. Giusti, *J. Agric. Food Chem.* **55**, 4443 (2007).
- [57] K. Wongcharee, V. Meeyoo, and S. Chavadej, *Sol. Energy Mater. Sol. Cells* **91**, 566–571 (2007).
- [58] W. R. Duncan and O. V. Prezhdo, *Annu. Rev. Phys. Chem.* **58**, 143 (2007).
- [59] S. Meng, J. Ren, and E. Kaxiras, *Nano Lett.* **8**, 3266–3272 (2008).
- [60] G. Calogero and G. Di Marco, *Sol. Energy Mater. Sol. C* **92**, 1341–1346 (2008).
- [61] A. Calzolari, D. Varsano, A. Ruini, A. Catellani, R. Tel-Vered, H. B. Yildiz, O. Ovits, and I. Willner, *J. Phys. Chem. A* , **113**, 8801–8810 (2009).
- [62] S. Furukawa, H. Iino, T. Iwamoto, K. Kukita, and S. Yamauchi, *Thin Solid Films* **518**, 526–529 (2009).
- [63] P. Luo, H. Niu, G. Zheng, X. Bai, M. Zhang, and W. Wang, *Spectrochim. Acta Part A* **74**, 936–942 (2009).
- [64] H. Chang and Y.J. Lo, *Sol. Energy* **84**, 1833–1837 (2010).
- [65] H. Zhou, L. Wu, Y. Gao, and T. Ma, *J. Photochem. and Photobio. A: Chemistry* **219**, 188–194 (2011).
- [66] M. H. Buraidah, L. P. Teo, S. N. F. Yusuf, M. M. Noor, M. Z. Kufian, M. A. Careem, S. R. Majid, R. M. Taha, and A. K. Arof, *Int. J. Photoenergy*, **2011**, 273683 (2011).
- [67] K. A. Aduloju and M.B. Shitta, *Int. J. Phys. Sci.* **7**, 709–712 (2012).
- [68] G. Calogero, J.H. Yum, A. Sinopoli, G. Di Marco, M. Grätzel, and M. K. Nazeeruddin, *Sol. Energy* **86**, 1563–1575 (2012).
- [69] C.-Y. Chien and B.-D. Hsu, *Solar Energy* **98**, 203–211 (2013).
- [70] P. E. Blöchl, *Phys. Rev. B* **50**, 17953 (1994).
- [71] G. Kresse and J. Hafner, *Phys. Rev. B* **47**, 558 (1993).
- [72] G. Kresse and J. Joubert, *Phys. Rev. B* **59**, 1758 (1999).
- [73] J. P. Perdew, K. Burke, and M. Ernzerhof, *Phys. Rev. Lett.* **77**, 3865 (1996).
- [74] J. Heyd, G. E. Scuseria, and M. Ernzerhof, *J. Chem. Phys.* **118**, 8207 (2003).
- [75] J. Heyd, G. E. Scuseria, and M. Ernzerhof, *J. Chem. Phys.* **124**, 219906 (2006).
- [76] J. Paier, M. Marsman, K. Hummer, G. Kress, I. C. Gerber, and J. G. Angyan, *J. Chem. Phys.* **125**, 249901 (2006).
- [77] A. Janotti, J. B. Varley, P. Rinke, N. Umezawa, G. Kresse, and C. G. Van de Walle, *Phys. Rev. B* **81**, 085212 (2010).
- [78] V. Çelik and E. Mete, *Phys. Rev. B* **86**, 205112 (2012).
- [79] J. P. Perdew, M. Ernzerhof, and K. Burke, *J. Chem. Phys.* **105**, 9982 (1996).
- [80] M. Gajdoš, K. Hummer, G. Kresse, J. Furthmüller, and F. Bechstedt, *Phys. Rev. B* **73**, 045112 (2006).
- [81] H. Ünal, O. Gülseren, Ş. Ellialtıođlu, and E. Mete, *Phys. Rev. B* **89**, 205127 (2014).
- [82] D. Gunceler, K. Letchworth-Weaver, R. Sundararaman, K.A. Schwarz, and T.A. Arias, *Modelling Simul. Mater. Sci. Eng.* **21**, 074005 (2013).
- [83] R. Sundararaman, D. Gunceler, K. Letchworth-Weaver, and T. A. Arias. *JDFTx*. <http://jdfdx.sourceforge.net> (2012).
- [84] R. Sundararaman, D. Gunceler, T. A. Arias - *J. Chem. Phys.*, **141**, 134105 (2014).
- [85] D. Gunceler, T. A. Arias - under review - arXiv preprint at arXiv:1403.6465, (2014).